

# News on the slow neutron capture process in AGB stars

Diego Vescovi<sup>1,\*</sup>

<sup>1</sup>Goethe University Frankfurt, Max-von-Laue-Strasse 1, Frankfurt am Main 60438, Germany

**Abstract.** Asymptotic giant branch (AGB) stars are responsible for the production of the main component of the solar s-process distribution. Despite enormous progress in the theoretical modeling of these objects over the last few decades, many uncertainties remain. The still-unknown mechanism leading to the production of  $^{13}\text{C}$  neutron source is one example. The nucleosynthetic signature of AGB stars can be examined in a number of stellar sources, from spectroscopic observations of intrinsic and extrinsic stars to the heavy-element isotopic composition of presolar grains found in meteorites. The wealth of available observational data allows for constraining the processes occurring in AGB interiors. In this view, we discuss recent results from new AGB models including the effects of mixing triggered by magnetic fields, and show comparisons of the related s-process nucleosynthesis with available observations.

## 1 Introduction

Asymptotic giant branch (AGB) stars are known to be one of the main producers of carbon, nitrogen, fluorine, and about half of the elements heavier than strontium, thus contributing greatly to the chemical enrichment of the Universe [1]. These stars are characterized by recurrent thermal instabilities of the He-burning shell, known as thermal pulses (TPs), which interrupt the quiescent shell-H burning that dominates the nuclear energy generation for thousands of years during the interpulse phase. H- and He-burning products can be carried up to the stellar surface by episodes of convective mixing, possibly occurring after each thermal pulse, known as third dredge-up (TDU) events. These are responsible for the formation of carbon stars and the surface enrichment of heavy elements, produced in stellar interiors by the slow neutron capture process (s-process) in low-mass AGB stars ( $M \lesssim 3M_{\odot}$ ) [2].

In these objects, the main neutron source is the  $^{13}\text{C}(\alpha, n)^{16}\text{O}$  reaction [3, 4], while the  $^{22}\text{Ne}(\alpha, n)^{25}\text{Mg}$  reaction is only marginally activated during the TPs [5]. For the  $^{13}\text{C}(\alpha, n)^{16}\text{O}$  reaction to effectively operate, some  $^{13}\text{C}$  must be present in the He-rich zone located below the H-rich convective envelope. Its synthesis requires the penetration of a small quantity of protons below the envelope itself, where they are captured by the abundant  $^{12}\text{C}$  thus forming a  $^{13}\text{C}$  pocket. To date, the mechanism responsible for the creation of the  $^{13}\text{C}$  pocket remains one of the major unknowns in the modeling of AGB stars and the main uncertainty in the relative nucleosynthesis of heavy elements through the s-process [6]. Over the past few years, many physical mechanisms for the partial mixing of H-rich material from the convective envelope have been investigated, as induced by convective overshoot [7, 8], rotation [9, 10], internal gravity waves [11, 12], and magnetic fields [13–15].

---

\*e-mail: [vescovi@iap.uni-frankfurt.de](mailto:vescovi@iap.uni-frankfurt.de)

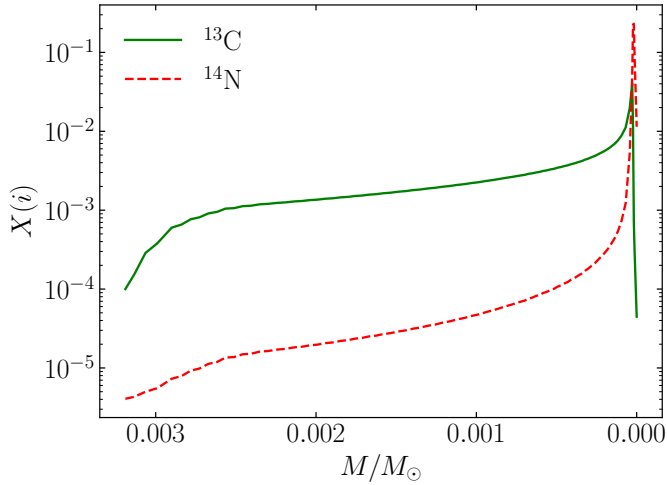


**Figure 1.**  $^{13}\text{C}$  and  $^{14}\text{N}$  abundance in the  $^{13}\text{C}$  pocket region for FRUITY Magnetic models.

Because the s-process affects a large number of observable and is dependent on only a few fundamental quantities (such as neutron density, total neutron flux, and the cross sections of nuclei with a magic number of neutrons) [16], observational constraints for AGB stars are useful in distinguishing between suitable mechanisms. Here, we consider new theoretical predictions from FRUITY stellar models accounting for a magnetically-induced  $^{13}\text{C}$  pocket and show their capability of reproducing observational constraints, as provided by the analysis of presolar stellar dust grains, spectroscopic observations of intrinsic and extrinsic AGB stars, and the chemical properties of Galactic open clusters.

## 2 Stellar magnetic models and observations

Magnetic fields may play an important role in the transport of angular momentum and chemical elements during stellar evolution [17]. In this regard, the buoyancy of material supported by magnetic pressure was shown to be an efficient physical mechanism for the transport of material from radiative regions to the convective envelope in low-mass giants stars [18] and provide a sufficient mass transport rate to explain the formation of the  $^{13}\text{C}$  pocket in TP-AGB stars [13]. The inclusion of magnetic mixing in the FUNS evolutionary code was recently done by [19] to generate a new set of FRUITY stellar models [20]. According to these models, the action of magnetic mixing results in deep penetration of a relatively small number of protons, that are almost entirely consumed for the synthesis of  $^{13}\text{C}$ . As a consequence, the local generation of  $^{14}\text{N}$  through the p-captures on  $^{13}\text{C}$  nuclei is greatly suppressed (see Figure 1). A  $^{13}\text{C}$  reservoir with these characteristics, i.e. extended (a few  $10^{-3} M_{\odot}$ ) and with low concentrations of  $^{13}\text{C}$ , was shown to be suitable in reproducing the distributions of s-process isotopes and elements, as measured in presolar silicon carbide (SiC) grains [21]. In particular, the mainstream (MS) ones, which account for about 90% of all SiC grains, are believed to have originated from carbon AGB stars and show their nucleosynthetic signature [22]. Therefore, isotope ratios of heavy elements measured in MS SiC grains are commonly used to study the s-process occurring in AGB stars and provide constraints on AGB stellar models [23–26]. Most of the presolar MS SiC grains have been shown to originate from AGB stars with  $M \sim 2 M_{\odot}$  and close-to-solar metallicity [27, 28]. FRUITY Magnetic models

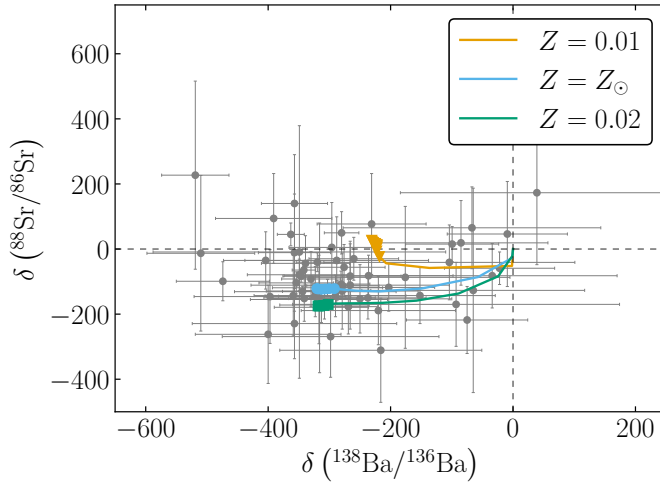


**Figure 2.** Comparison between FRUITY Magnetic  $2 M_{\odot}$  models at different metallicities and presolar grain isotope ratios. Isotope ratios are reported in the conventional  $\delta$  notation, defined as the deviation of the ratio measured in a grain relative to the terrestrial value in parts per thousand. Grain data are from the PGD database [29].

within this mass and metallicity range, once properly calibrated, can accurately reproduce MS SiC grain isotope ratios for heavy elements [19] and, in particular, the negative  $\delta$ -values of  $^{88}\text{Sr}/^{86}\text{Sr}$  and  $^{138}\text{Ba}/^{136}\text{Ba}$  ratios showed by the bulk of the data (see Figure 2).

The shortage of primary  $^{14}\text{N}$  predicted by FRUITY Magnetic models has significant implications on the synthesis of light elements whose production involves nitrogen, including fluorine. In AGB stars, fluorine is synthesized via the reactions chain  $^{14}\text{N}(n, p)^{14}\text{C}(\alpha, \gamma)^{18}\text{O}(p, \alpha)^{15}\text{N}(\alpha, \gamma)^{19}\text{F}$  [30]. Nitrogen and free neutrons are therefore simultaneously required to start the chain. The latter are provided by the activation of the  $^{13}\text{C}(\alpha, n)^{16}\text{O}$  reaction. During the radiative burning of the  $^{13}\text{C}$  pocket, the freshly synthesized neutrons are consumed together with the  $^{14}\text{N}$  present in the He-intershell to produce  $^{15}\text{N}$ , which is then burnt to create  $^{19}\text{F}$  in the following convective TP. A second source of fluorine descends from the amount of  $^{13}\text{C}$  and  $^{14}\text{N}$  left in H-burning ashes (plus some eventual un-burnt  $^{13}\text{C}$  in the pocket [8]) engulfed and burnt in the convective TP. Fluorine is then transported to the surface by convective processes during the following TDU. As a consequence, the abundance of  $^{19}\text{F}$  in the envelope is expected to correlate with that of carbon and s-process elements. Direct evidence of fluorine production in AGB stars is provided by spectroscopic observations of photospheric  $[\text{F}/\text{Fe}]$  enhancements in both intrinsic and extrinsic stellar objects (see [31] and references therein). As shown in Figure 3, FRUITY Magnetic models predictions for low-mass AGB stars provide a good agreement for the F-enhancement trend with the metallicity. Even more interesting, these models are able to reproduce the observed spread for  $[\text{F}/\text{s}]$  vs.  $[\text{s}/\text{Fe}]$  ratios. Due to the shortage of  $^{14}\text{N}$  in the  $^{13}\text{C}$  pocket region, the fluorine production is dominated by the amount of  $^{13}\text{C}$  and  $^{14}\text{N}$  in the H-burning ashes [20]. As a result, the predicted fluorine envelope abundance is significantly reduced with respect to models exhibiting a large production of fluorine from primary  $^{14}\text{N}$  [31].

Stellar yields from AGB stars are key ingredients to model the Galactic chemical evolution (GCE) and for interpreting the solar s-process distribution [1]. Additional precious information, regarding the chemical properties of the Galactic disk and its evolution, comes

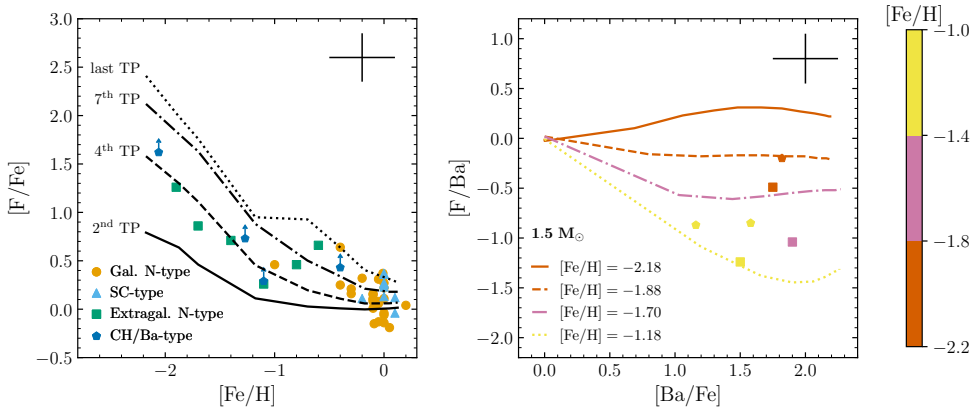


**Figure 3.** (Left panel) Comparison between observed [F/Fe] ratios as a function of the metallicity and FRUITY Magnetic models. Symbols refer to four data groups: circles, galactic (N-type) carbon stars; triangles, SC-type stars; squares, extragalactic carbon stars; pentagons, extrinsic CH/Ba stars. Lines represent theoretical predictions for 2 (for  $[\text{Fe}/\text{H}] \geq -0.7$ ) and  $1.5 M_{\odot}$  (for  $[\text{Fe}/\text{H}] < -0.7$ ) AGB stars at different thermal pulses (TPs). (Right panel) [F/Ba] vs. [Ba/Fe] in the sample stars with  $[\text{Fe}/\text{H}] \leq -1.0$ . Data points and theoretical lines are color-coded by [Fe/H]. Typical error bars are indicated.

from the study of open clusters. The latest observational data from the final release of the Gaia-ESO survey, show that there is an increasing, albeit weak, trend in the production of s-process elements as the cluster age decreases, but with radial variations, with respect to the center of the Galaxy [32]. These are related to the metallicity dependence of the stellar yields of the s-process and the radial dependence of the star formation history [33]. Specifically, in the inner part of the Galactic disk, the average  $[\text{s}/\text{Fe}]$  gradient does not vary significantly with age, thus indicating a substantial decrease of the s-process efficiency at the super-solar metallicity characteristic of the innermost part of the disk, as expected by the secondary nature of the s-process [2]. Nonetheless, GCE computations adopting AGB stellar yields from past FRUITY models overestimate the production of the s-process elements for clusters located at Galactocentric distances  $R_{\text{GC}} < 7$  kpc [34]. Conversely, FRUITY Magnetic models are characterized by a lower neutron-to-seed ratio, due to the low  $^{13}\text{C}$  concentration in the pocket (see Figure 1), so that lower neutron fluxes and s-process enhancements are attained at relatively high metallicity. In this regard, the behavior of neutron-capture elements in the inner Galactic disk is well explained by the current FRUITY Magnetic models [33].

### 3 Conclusions

In recent years, significant progress has been made in determining the evolution and nucleosynthesis of AGB stars. One of the lingering questions is the physical mechanism leading to the formation of the  $^{13}\text{C}$  pocket in these stars. Among the various theories, mixing caused by magnetic instabilities has been shown to be a viable solution. In this work, we discussed a new set of FRUITY models that account for magnetic-buoyancy-induced mixing. These models provide a useful theoretical tool for explaining several observable constraints, such as heavy-element isotope ratios measured in presolar MS SiC grains, fluorine enhancements of AGB stars, and s-element abundances in galactic open clusters. These findings support the magnetic mixing as the potential mechanism behind the activation of the  $^{13}\text{C}$  neutron source

in AGB stars. Nonetheless, further analyses are required for a definite claim, including more comparisons with s-process enriched objects such as barium stars and post-AGB stars, as well as targeted multidimensional magnetohydrodynamic simulations.

DV acknowledges financial support from the German-Israeli Foundation (GIF No. I-1500-303.7/2019).

## References

- [1] N. Prantzos, C. Abia, Limongi et al., *MNRAS* **476**, 3432 (2018), 1802.02824
- [2] M. Busso, R. Gallino, G.J. Wasserburg, *ARA&A* **37**, 239 (1999)
- [3] O. Straniero, R. Gallino, M. Busso et al., *ApJL* **440**, L85 (1995)
- [4] S. Cristallo, M. La Cognata, C. Massimi et al., *ApJ* **859**, 105 (2018), 1804.10751
- [5] O. Straniero, A. Chieffi, M. Limongi et al., *ApJ* **478**, 332 (1997)
- [6] F. Herwig, *ARA&A* **43**, 435 (2005)
- [7] F. Herwig, T. Bloeker, D. Schoenberner et al., *A&A* **324**, L81 (1997)
- [8] S. Cristallo, O. Straniero, R. Gallino et al., *ApJ* **696**, 797 (2009), 0902.0243
- [9] F. Herwig, N. Langer, M. Lugaro, *ApJ* **593**, 1056 (2003), astro-ph/0305491
- [10] L. Siess, S. Goriely, N. Langer, *A&A* **415**, 1089 (2004)
- [11] P.A. Denissenkov, C.A. Tout, *MNRAS* **340**, 722 (2003)
- [12] U. Battino, M. Pignatari, C. Ritter et al., *ApJ* **827**, 30 (2016), 1605.06159
- [13] O. Trippella, M. Busso, S. Palmerini et al., *ApJ* **818**, 125 (2016), 1512.06777
- [14] D. Vescovi, M. Busso, S. Palmerini, et al., *ApJ* **863**, 115 (2018), 1807.01058
- [15] M. Busso, D. Vescovi, S. Palmerini et al., *ApJ* **908**, 55 (2021), 2011.07469
- [16] F. Käppeler, R. Gallino, S. Bisterzo et al., *Reviews of Modern Physics* **83**, 157 (2011)
- [17] A. Maeder, *Physics, Formation and Evolution of Rotating Stars* (Springer-Verlag Berlin Heidelberg, 2009)
- [18] M. Busso, G.J. Wasserburg, K.M. Nollett et al., *ApJ* **671**, 802 (2007), 0708.2949
- [19] D. Vescovi, S. Cristallo, M. Busso, N. Liu, *ApJL* **897**, L25 (2020), 2006.13729
- [20] D. Vescovi, S. Cristallo, S. Palmerini et al., *A&A* **652**, A100 (2021), 2106.08241
- [21] N. Liu, M.R. Savina, R. Gallino et al., *ApJ* **803**, 12 (2015), 1501.05883
- [22] L.R. Nittler, F. Ciesla, *ARA&A* **54**, 53 (2016)
- [23] S. Palmerini, M. Busso, D. Vescovi et al., *ApJ* **921**, 7 (2021), 2107.12037
- [24] N. Liu, S. Cristallo, D. Vescovi, *Universe* **8**, 362 (2022), 2206.13721
- [25] S. Taioli, D. Vescovi, M. Busso et al., *ApJ* **933**, 158 (2022), 2109.14230
- [26] N. Liu, T. Stephan, S. Cristallo et al., arXiv e-prints arXiv:2209.10347 (2022)
- [27] H.P. Gail, S.V. Zhukovska, P. Hoppe, M. Tieloff, *ApJ* **698**, 1136 (2009)
- [28] S. Cristallo, A. Nanni, G. Cescutti et al., *A&A* **644**, A8 (2020), 2010.08268
- [29] T. Stephan, M. Bose, A. Boujibar et al., *The Presolar Grain Database Reloaded - Silicon Carbide*, in *51st Annual Lunar and Planetary Science Conference* (2020), Lunar and Planetary Science Conference, p. 2140
- [30] M. Forestini, S. Goriely, A. Jorissen, M. Arnould, *A&A* **261**, 157 (1992)
- [31] C. Abia, S. Cristallo, K. Cunha, P. de Laverny, V.V. Smith, *A&A* **625**, A40 (2019)
- [32] L. Magrini, C. Viscasillas Vazquez, L. Spina et al., arXiv e-prints arXiv:2210.15525 (2022), 2210.15525
- [33] L. Magrini, D. Vescovi, G. Casali et al., *A&A* **646**, L2 (2021), 2101.04429
- [34] G. Casali, L. Spina, L. Magrini et al., *A&A* **639**, A127 (2020), 2006.05763